ChemComm

COMMUNICATION

Check for updates

Efficient CO_2 photoreduction using a water-soluble conjugated polyelectrolyte grafted imidazolium-functionalized side chain†

Mantao Chen,[a] Waner Li,[a] Tingting Zhang,[a] Tianjing Xu,[b] Bo Wang,[a] Chao Zeng, [ID][c] Fei Li [ID] *[b] and Chunhui Dai [ID] *[a]

Herein, we reported the development of a water-soluble conjugated polyelectrolyte (CPE) for efficient CO_2 photoreduction under visible light ($\lambda > 420$ nm). Bearing a fluorene-benzothiadiazole backbone and imidazolium-functionalized side chains, PFBT-Im exhibits remarkable photocatalytic activity with nearly 100% selectivity and a CO yield of 453.16 µmol g^{-1} within 4 h, which is 8.6 and 2.5 times larger than those of conjugated polymers grafted with octyl and trimethylammonium side chains, respectively.

The dramatic consumption of fossil fuels and ever-increasing CO_2 emission have resulted in the world-wide energy crisis and climate warming issue. In this context, the development of CO_2 neutralization technology is drawing enormous scientific attention. Photocatalytic reduction of CO_2 into carbonaceous products offers great potential in recycling CO_2 sustainably, which can not only reduce the concentration of CO_2 in air but can also produce valuable chemical fuels simultaneously, such as CO, CH_4, CH_3OH, *etc.*[1–3] As promising alternatives to traditional inorganic semiconductors, organic conjugated polymers (CPs) have attracted massive attention due to their inherent properties of light weight, earth-abundant nature, and facile functionalization at the molecular level.[4,5] During the past ten years, a large number of polymer photocatalysts have been developed and proposed for efficient CO_2 photoreduction, like graphitic carbon nitride (g-C_3N_4),[6] conjugated microporous polymers (CMPs),[7] covalent organic frameworks (COFs),[8] covalent triazine frameworks (CTFs),[9] *etc.* Despite certain progress achieved,

in most cases, these highly crosslinking polymer photocatalysts with large particle sizes suffer from inadequate light harvesting, relatively low surface areas, and bulk recombination of photogenerated charges, which severely restrict their CO_2 photoreduction activities. To address these problems, it is urgently needed to explore highly active nano-polymer photocatalysts for CO_2 reduction.

Conjugated polyelectrolytes (CPEs) are an important class of charged macromolecules consisting of π-delocalized conjugated backbones and pendant ionic side chains. The last two decades have witnessed the wide application of CPEs in photovoltaic cells, biological imaging and therapy, photocatalytic water splitting, organic light-emitting diodes (OLEDs), *etc.*[10–12] The π-conjugated backbones offer CPEs special properties, such as strong light-harvesting properties, variable energy levels, and remarkable chemical stability. Compared to their neutral counterparts, CPEs with pendant ionic functionalities are typically endowed with water dispersity, enhanced ionic conductivity, excellent redox activities, and stabilization of charge carriers through electrostatic interactions. These structural features of CPEs allow the facile creation of a homogeneous photocatalytic system for CO_2 conversion. In particular, ionized groups in these CPEs may form a strong dipole interaction at the interface between the polyelectrolyte and CO_2 molecules. This in turn enhances the activation of CO_2 molecules and thus the photocatalytic activity of the polyelectrolyte. In spite of these advantages, to the best of our knowledge, CPEs have never been applied for CO_2 photoreduction so far.
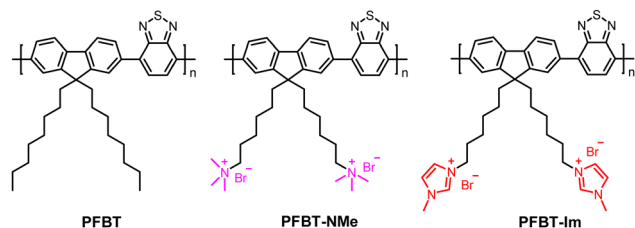
Recent studies have revealed that the incorporation of imidazolium into the polymer backbone could dramatically improve the adsorption and activation of CO_2. A great variety of heterogeneous polymer catalysts for CO_2 fixation have been constructed by introducing imidazolium moieties into chitosan,[13] polyampholytes,[14] coordinated porous polymers (CPPs),[15] and covalent organic frameworks (COFs).[16] Inspired by this, we grafted an imidazolium side chain into the polymer backbone to improve the water dispersibility of the polymer and also the interaction between CO_2 and the polymer chain. Fluorene-2,1,3-benzothiadiazole, which has been demonstrated as an active unit for CO_2-to-CO conversion in previous

[a] Jiangxi Key Laboratory for Mass Spectrometry and Instrumentation, School of Chemistry and Materials Science, East China University of Technology, Nanchang 330013, P. R. China. E-mail: chunh-dai@ecut.edu.cn

[b] National R&D Center for Chinese Herbal Medicine Processing, College of Engineering, China Pharmaceutical University, Nanjing 211109, China. E-mail: fei.li@cpu.edu.cn

[c] School of Chemical Engineering, Jiangxi Normal University, Nanchang 330022, China

Scheme 1   Chemical structures of PFBT, PFBT–NMe and PFBT–Im.

Fig. 1   (a) UV-vis absorption spectra of PFBT in THF and PFBT–NMe and PFBT–Im in CH$_3$OH. (b) The energy level diagram of the three polymers. DLS results of (c) PFBT–NMe and (d) PFBT–Im in H$_2$O (insets are the TEM images of polyelectrolyte nanoaggregates).

reports,[17,18] was employed as a polymer backbone. The resulting polyelectrolyte, namely PFBT-Im, exhibited efficient photocatalytic activity for CO$_2$ reduction without loading metal cocatalysts in aqueous solution using dimethylamine (Et$_2$N) as the sacrificial agent under visible light (Scheme 1). To examine the impact of side chains on the CO$_2$ photoreduction activity of the polymer, other two polymers having the same backbone, PFBT-NMe$_3$ with cationic trimethylammonium substituents and PFBT with alkyl side chains are also developed. Compared to the neutral polymer, PFBT-NMe and PFBT-Im showed 8.6- and 2.5-fold improvement in the CO yield under identical photocatalytic conditions.

The synthetic procedures for cationic monomers and polyelectrolytes are shown in Scheme S1. Both PFBT-NMe and PFBT-Im were prepared by one-step Suzuki polymerization between 4,7-bis(4,4,5,5-tetramethyl-1,3,2-dioxaborolan-2-yl)-2,1,3-benzothiadiazole with 6,6′-(2,7-dibromo-9H-fluorene-9,9-diyl)bis(N,N,N-trimethylhexan-1-aminium) dibromide (M1) and 3,3′-((2,7-dibromo-9H-fluorene-9,9-diyl)bis(hexane-6,1-diyl))bis(1-methyl-1H-imidazol-3-ium) dibromide (M2), respectively. This direct coupling method renders fully ionized side chains in the polymer chain for both polyelectrolytes with high isolated yields above 85%. The chemical structures of the monomers and polyelectrolytes were characterised by ^{1}H nuclear magnetic resonance (NMR) spectroscopy (Fig. S1–S4, ESI†) and Fourier transform infrared (FTIR) spectroscopy.[19] The ^{1}H NMR spectrum of PFBT-NMe exhibits a characteristic peak of the pendent trimethylammonium unit (3.01 ppm) at the 9-position of fluorene.[10,20] The spectrum of PFBT-Im features aromatic resonances in the range of 7.44–8.54 ppm due to the benzene and imidazolium unit, as well as a single peak at 3.61 ppm ascribed to the methyl group attached in the imidazolium.[20] The FTIR spectrum shows vibration peaks attributed to the methylene group at 2928 and 2851 cm^{-1} for both PFBT-NMe and PFBT-Im (Fig. S5, ESI†). In addition, PFBT-NMe exhibits a stretching band for the terminal CH$_3$ at 3397 cm^{-1}, and the characteristic peaks of the ionized imidazole moiety at 3091 and 1161 cm^{-1} were found for PFBT-Im.[16] PFBT is well soluble in low-polar organic solvents, while PFBT-NMe and PFBT-Im possess good solubility in polar solvents like alcohol and water.

Fig. 1a displays the UV-vis absorption spectra of PFBT, PFBT-NMe, and PFBT-Im in solution. Bearing the same polymer backbone, the three polymers showed strong light absorption in the visible region. Based on the absorption edge of the polymer film (Fig. S6, ESI†), the optical gaps of roughly 2.40, 2.36, and 2.34 eV were estimated for PFBT, PFBT-NMe and PFBT-Im, respectively. To determine the energy levels of the polymers, cyclic voltammograms (CVs) of drop-cast polymer
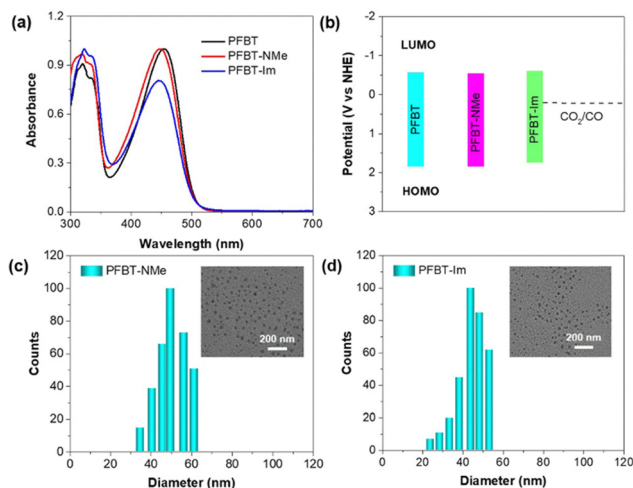
samples on glassy carbon electrodes were collected and the results are presented in Fig. S7 (ESI†). The lowest unoccupied molecular orbital (LUMO) and highest occupied molecular orbital (HOMO) energy levels are −0.58/1.82, −0.54/1.82, and −0.61/1.73 eV for PFBT, PFBT-NMe and PFBT-Im, respectively (Fig. 1b). The high-lying LUMO levels of the polymers are much higher than the redox potential of CO$_2$/CO, indicating a thermodynamically sufficient driving force for all polymers to enable CO$_2$ reduction under light irradiation. The morphology of polyelectrolyte aggregates in H$_2$O was studied by transmission electron microscopy (TEM) and the size distribution was analyzed by dynamic light scattering (DLS). The TEM image shows that both polyelectrolytes can form spherical nanoparticles and the average sizes of PFBT-NMe and PFBT-Im nanoparticles are ∼41 nm and 38 nm, respectively. DLS measurements show that all resulting nanoparticles have a narrow particle size distribution and the average hydrodynamic diameters of PFBT-NMe and PFBT-Im are 49.5 nm and 43.8 nm, respectively (Fig. 1c and d). Compared to bulk PFBT, the small size of the polyelectrolyte aggregate in water for PFBT-NMe and PFBT-Im facilitates the diffusion of photoinduced excitons to the interface between the polymer photocatalyst and CO$_2$, which thus promotes the photocatalytic CO$_2$ reduction.[21]

Under the excitation of 375 nm, PFBT exhibited a strong emission peak at 556 nm, which was red-shifted to 571 nm for PFBT-NMe and 568 nm for PFBT-Im, respectively (Fig. 2a). Notably, as compared to PFBT, the fluorescence intensity of PFBT-NMe was apparently lower and the weakest emission was observed for PFBT-Im, implying the improved charge transport ability of PFBT-Im during the photocatalytic reaction. Besides, the time-resolved fluorescence spectra show that the fluorescence decay lifetimes in the polymers are on the nanosecond scale. The average lifetimes from double exponential function fitting are 1.89, 2.55 and 4.66 ns for PTBT, PFBT-NMe and PFBT-Im, respectively (Fig. 2b and Fig. S8, ESI†). The longer
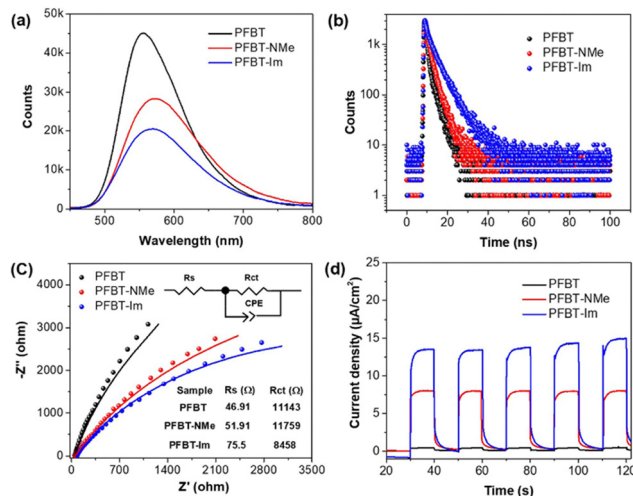
Fig. 2 (a) Photoluminescence and (b) fluorescence decay traces (λ_{ex} = 375 nm) of the polymers. (c) EIS Nyquist plots and (d) transient photocurrent responses of the polymer electrodes (>420 nm).
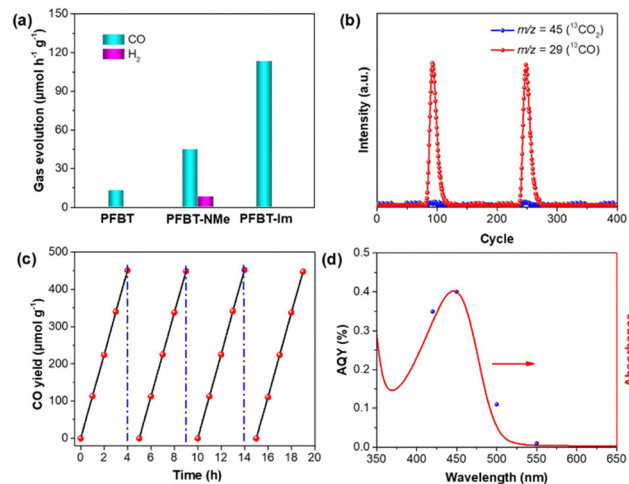

Fig. 3 (a) The time−yield plots of the gas products using as-prepared polymers under visible light irradiation (>420 nm). (b) GC–MS analysis of PFBT-Im in the $^{13}CO_2$ isotope experiment. (c) CO yield of PFBT-Im in cycling stability tests. (d) UV-vis absorption spectrum and the AQY plots of PFBT-Im.

excited-state lifetime of PFBT-Im indicates that the charge recombination in the polymer is greatly inhibited and thus is beneficial for achieving better photocatalytic performance.

To gain insight into the charge-transport behaviors of the as-synthesized polymers, electrochemical impedance spectroscopy (EIS) and a visible-light photocurrent response study using a typical three-electrode cell were further conducted. The diameter of semicircular Nyquist plots of PFBT-Im at high frequencies is smaller than those of PFBT and PFBT-NMe (Fig. 2c and Table S1, ESI†), indicating a reduced charge-transfer resistance and the highest charge separation efficiency.[22,23] In addition, as compared to PFBT and PFBT-NMe, a larger photocurrent response was observed for PFBT-Im upon on/off visible light irradiation (Fig. 2d). The enhanced photocurrent in the PFBT-Im electrode clearly validates that the photoinduced charge carriers inside PFBT-Im are more strongly promoted than those in PFBT and PFBT-NMe, which eventually boosts the CO_2 photoreduction performance.

The CO_2 photoreduction performance of the as-prepared polymers was evaluated in a CO_2-saturated aqueous solution with diethylamine (DEA) as the sacrificial agent under mild conditions (30 °C, 1 atm CO_2). Attached ionic side chains in the polymer backbone, PFBT-NMe and PFBT-Im showed excellent dispersity in the photocatalytic solution, while those in the neutral PFBT are poorly dispersed (Fig. S9, ESI†). After irradiation with visible light (>420 nm) for 2 h, PFBT exhibits low CO_2 reduction efficiency with a CO evolution rate of 13.12 μmol h^{-1} g^{-1} (Fig. 3a). By comparison, PFBT-NMe exhibits a significantly enhanced CO yield of 44.69 μmol h^{-1} g^{-1}, which is about 3.4 times higher than that of PFBT. Furthermore, H_2 originating from water reduction was also detected with a yield of 8.17 μmol h^{-1} g^{-1}. When using the PFBT-Im grafted imidazolium-functionalized side chain as the photocatalyst, the water reduction is completely inhibited and the catalytic system displays the highest CO yield of 113.29 μmol h^{-1} g^{-1} with an impressive reaction selectivity of nearly 100%. The main reason for the greatly

improved photoactivity of PFBT-Im compared to those of PFBT and PFBT-NMe is likely the synergistic effect of the enhanced interface interaction between the polymer and CO_2 and water dispersity, as well as the boosted transport of charge carriers during photocatalysis. Actually, the CO yield of PFBT-Im for the photocatalytic CO_2 conversion is superior to that of most of the polymer nanomaterials reported so far under similar experimental conditions (Table S2, ESI†), which is likely attributed to the strong light absorption, excellent water solubility and specific active sites for the CO_2 activation of PFBT-Im.[6,24–26]

To verify the CO_2-to-CO conversion catalyzed by the polymer photocatalysts, several additional control experiments using PFBT-Im as the photocatalyst were conducted (Fig. S10, ESI†). Photocatalytic reactions performed without light or the photocatalyst did not result in any products. Under the same illumination conditions, further experiments under a N_2-saturated atmosphere gave no CO. These results suggested that the evolved CO is indeed from the reduction of CO_2 triggered by the photocatalysts and light irradiation. Besides, extremely low photoactivity was measured without adding H_2O, which is likely due to the presence of trace water in Et_2N. In the isotopic experiments using $^{13}CO_2$ as a reactant, the ^{13}CO signal appeared at m/z = 29 in gas chromatography and mass spectrometry (GC-MS) confirmed the formation of ^{13}CO after the photocatalytic reaction (Fig. 3b). This observation further indicates that CO is generated from the CO_2 photoreduction on PFBT-Im.

Photocatalytic CO_2 reduction of PFBT-Im was then investigated using alternative sacrificial agents under identical illumination conditions (Fig. S11, ESI†). In Et_3N and 10 vol% TEOA, PFBT-Im displayed lower activities, with CO evolution rates of 59.45 and 31.97 μmol h^{-1} g^{-1}, respectively. Besides, PFBT-Im had a CO yield of 21.68 μmol h^{-1} g^{-1} using ascorbic acid (AA) as a sacrificial agent, while the CO yield declined to 13.51 μmol h^{-1} g^{-1} in EDTA-2Na aqueous solution. These results indicate that Et_2N is the optimized sacrificial agent for PFBT-Im to drive the CO_2 photoreduction.

The photocatalytic cyclability and stability of PFBT-Im was evaluated by performing the photocatalytic experiments with four consecutive runs. After each run, the reaction mixture was purged with fresh CO_2 and irradiated for 4 h. As shown in Fig. 3d, the CO evolution of PFBT-Im almost remains unchanged even after four successive cycles. Moreover, TEM measurements (Fig. S12, ESI†) and the FTIR (Fig. S13, ESI†) and ^{1}H NMR (Fig. S14, ESI†) spectra reveal no noticeable change in the chemical structure and morphology of the recycled photocatalyst, revealing the extremely high photostability of PFBT-Im.

PFBT-Im has the highest apparent quantum yield (AQY) of 0.40% at 450 nm, and the values significantly decreased to 0.11% and 0.01% at 500 and 550 nm, respectively (Fig. 3d). This trend in AQY values is consistent with its UV-vis absorption spectra and the results imply that the photons contributing to the photocatalytic CO evolution are mainly below 550 nm.

As is known, the CO_2 content in anthropogenic CO_2 emission, such as industrial flue gas, is very low ($\sim$15%).[27] In this regard, efficiently converting low-concentration CO_2 into value-added products is of significance, yet rarely reported. To examine the potential of PFBT-Im for CO_2 reduction in a real environment, we further conducted the photoreduction of CO_2 in an atmosphere of simulated flue gas. Under 4 h of irradiation with visible light ($>$420 nm), PFBT-Im offers a high CO yield up to 98.15 μmol h^{-1} g^{-1} and 100% reaction selectivity (Fig. S15, ESI†), outperforming many reported photocatalysts under similar conditions.[28–30]

In conclusion, we have developed a water-soluble conjugated polyelectrolyte grafted imidazolium-functionalized side chain for efficient CO_2 photoreduction under visible light ($>$420 nm). Taking advantage of its excellent water dispersity, strong interaction with CO_2 molecules and improved transport of photoinduced excitons, PFBT-Im exhibited a stable CO yield of 113.29 μmol h^{-1} g^{-1}, which is 8.6 and 2.5-fold improvement over those of alkyl and trimethylammonium-functionalized conjugated polymers. This contribution might pave a way for the further development of CPEs as a photocatalytic platform toward achieving highly efficient CO_2 conversion.

Data availability

The data supporting this article have been included as part of the ESI.†

Conflicts of interest

There are no conflicts to declare.

References

1 S. Lu, S. Zhang, Q. Liu, W. Wang, N. Hao, Y. Wang, Z. Li and D. Luo, *Carbon Neutralization*, 2024, **3**, 142–168.
2 L. Bao, S. Ali, C. Dai, Q. Zeng, C. Zeng, Y. Jia, X. Liu, P. Wang, X. Ren, T. Yang, M. Bououdina, Z.-H. Lu, Y. Wei, X. Yu and Y. Zhou, *ACS Nano*, 2024, **18**, 5878–5889.
3 W. Song, Y. Tang, B. Y. Moon, Q. Liao, H. Xu, Q. Hou, H. Zhang, D.-G. Yu, Y. Liao and I. Kim, *Green Chem.*, 2024, **26**, 2476–2504.
4 C. Dai and B. Liu, *Energy Environ. Sci.*, 2020, **13**, 24–52.
5 K. S. Song, P. W. Fritz and A. Coskun, *Chem. Soc. Rev.*, 2022, **51**, 9831–9852.
6 (a) Q. Xu, Z. Xia, J. Zhang, Z. Wei, Q. Guo, H. Jin, H. Tang, S. Li, X. Pan, Z. Su and S. Wang, *Carbon Energy*, 2022, **5**, 1–43; (b) H. Zhan, R. Zhou, K. Liu, Z. Ma, P. Wang, S. Zhan and Q. Zhou, *Sci. China Mater.*, 2024, **67**, 1740–1764.
7 (a) W. Wu, Z. Dong, M. Chen, W. Li, A. Liao, Q. Liu, Y. Zhang, Z. Zhou, C. Zeng, X. Gong and C. Dai, *Carbon Energy*, 2024, DOI: **10.1002/cey2.646**; (b) W. Wu, C. Feng, M. Chen, Q. Tan, Y. Deng, C. Zeng, L. Zhong and C. Dai, *Green Chem.*, 2023, **25**, 9335–9342.
8 (a) M. E. G. Carmo, L. Spies, G. N. Silva, O. F. Lopes, T. Bein, J. Schneider and A. O. T. Patrocinio, *J. Mater. Chem. A*, 2023, **11**, 13815–13843; (b) B. B. Rath, S. Krause and B. Valeska Lotsch, *Adv. Funct. Mater.*, 2024, **34**, 2309060.
9 (a) G. Liu, S. Liu, C. Lai, L. Qin, M. Zhang, Y. Li, M. Xu, D. Ma, F. Xu, S. Liu, M. Dai and Q. Chen, *Small*, 2024, **20**, 2307853; (b) A. Jana, A. Maity, A. Sarkar, B. Show, P. A. Bhobe and A. Bhunia, *J. Mater. Chem. A*, 2024, **12**, 5244–5253.
10 C. Dai, M. Panahandeh-Fard, X. Gong, C. Xue and B. Liu, *Sol. RRL*, 2019, **3**, 1800255.
11 Y. Bai, Z. Hu, J.-X. Jiang and F. Huang, *Chem. – Asian J.*, 2020, **15**, 1780.
12 Q. Che, J. Liu, Q. Chen, K. Zhao, B. Zhang, H. He, X. Wang, K. Wang and Y. Chen, *ACS Appl. Mater. Interfaces*, 2024, **16**, 19947–19956.
13 J. Sun, J. Wang, W. Cheng, J. Zhang, X. Li, S. Zhang and Y. She, *Green Chem.*, 2012, **14**, 654–660.
14 S. Soll, Q. Zhao, J. Weber and J. Yuan, *Chem. Mater.*, 2013, **25**, 3003–3010.
15 M. Bahadori, S. Tangestaninejad, M. Bertmer, M. Moghadam, V. Mirkhani, I. Mohammadpoor-Baltork, R. Kardanpour and F. Zadehahmadi, *ACS Sustainable Chem. Eng.*, 2019, **7**, 3962–3973.
16 L.-G. Ding, B.-J. Yao, F. Li, S.-C. Shi, N. Huang, H.-B. Yin, Q. Guan and Y.-B. Dong, *J. Mater. Chem. A*, 2019, **7**, 4689–4698.
17 B. Cai, M. Axelsson, S. Zhan, M. V. Pavliuk, S. Wang, J. Li and H. Tian, *Angew. Chem., Int. Ed.*, 2023, **62**, e202312276.
18 M. Chen, T. Xu, W. Wu, W. Li, C. Zeng, F. Li and C. Dai, *ACS Appl. Polym. Mater.*, 2024, **6**, 10875.
19 Z. Li, S. Shen, S. Hussain, B. Cui, J. Yao, Y. Su, Y. Wang, Y. Hao and R. Gao, *Anal. Chem.*, 2024, **96**, 5150–5159.
20 A. Parthasarathy, H. C. Pappas, E. H. Hill, Y. Huang, D. G. Whitten and K. S. Schanze, *ACS Appl. Mater. Interfaces*, 2015, **7**, 28027–28034.
21 H. Wang, S. Jin, X. Zhang and Y. Xie, *Angew. Chem., Int. Ed.*, 2020, **59**, 22828.
22 Z. Hu, Z. Wang, X. Zhang, H. Tang, X. Liu, F. Huang and Y. Cao, *iScience*, 2019, **13**, 33–42.
23 Y. Wu, X. Zhang, Y. Xing, Z. Hu, H. Tang, W. Luo, F. Huang and Y. Cao, *ACS Mater. Lett.*, 2019, **1**, 620–627.
24 S. N. Talapaneni, G. Singh, I. Y. Kim, K. AlBahily, A. H. Al-Muhtaseb, A. S. Karakoti, E. Tavakkoli and A. Vinu, *Adv. Mater.*, 2020, **32**, 1904635.
25 B. Cai, M. Axelsson, S. Zhan, M. V. Pavliuk, S. Wang, J. Li and H. Tian, *Angew. Chem., Int. Ed.*, 2023, **62**, e202312276.
26 Y. He, L. Yin, N. Yuan and G. Zhang, *Chem. Eng. J.*, 2024, **481**, 148754.
27 Z. Sun, Y. Liao, S. Zhao, X. Zhang, Q. Liu and X. Shi, *J. Mater. Chem. A*, 2022, **10**, 5174–5211.
28 C. Dai, L. Zhong, W. Wu, C. Zeng, Y. Deng and S. Li, *Sol. RRL*, 2022, **6**, 2100872.
29 M. Dong, J. Zhou, J. Zhong, H.-T. Li, C.-Y. Sun, Y.-D. Han, J.-N. Kou, Z.-H. Kang, X.-L. Wang and Z.-M. Su, *Adv. Funct. Mater.*, 2022, **32**, 2110136.
30 S. R. Chia, K. W. Chew, H. Y. Leong, S.-H. Ho, H. S. H. Munawaroh and P. L. Show, *Chem. Eng. J.*, 2021, **425**, 131436.